Capacitive-Coupling Inverter for PV Integration: Analysis and Implementation

ChenPei Zheng[1], NingYi Dai[1], ManChung Wong[1], ChiKong Wong[1], Miao Zhu[2]

1 Department of Electrical and Computer Engineering
University of Macau
Macao, SAR, P.R.China
E-mail:zhengchenp@163.com

2 Department of Electrical Engineering/ State Energy Smart Grid R&D Center
Shanghai Jiao Tong University (SJTU), China

Abstract—This paper presents a capacitive-coupling voltage source inverter (VSI) for single-phase grid connected photovoltaic (PV) system, which can achieve active power transfer and reactive power compensation simultaneously. The operation principle of the capacitive-coupling VSI was analyzed and compared with the conventional inductive-coupling VSI. Theoretical study indicates that capacitive-coupling grid-connected VSI can achieve the required power control with lower inverter voltage rating, which reduces the initial cost and operational losses. A single-phase PV integration system with capacitive-coupling VSI is implemented, in which a boost-half-bridge dc-dc converter is used. The boost-half-bridge dc-dc converter is selected due to its low cost, simple control method and high efficiency. The adaptive duty cycle control method for maximum power point tracking (MPPT) is used. The control system of the capacitive-coupling VSI is also implemented, which can transfer the active power from the dc converter to the ac grid and keep the dc-link voltage stable. Simulation results are provided to verify the validity of the capacitive-coupling VSI for PV integration. Comparison with inductive-coupling VSI is also done, which show that the capacitive-coupling VSI is able to transfer the same amount of power with a much lower dc-link voltage.

Keywords: Capacitive-coupling voltage source inverter, Inductive-coupling voltage source inverter, Maximum Power Point Tracking (MPPT)

I. INTRODUCTION

The concept of smart grid emerges as the times require, and in recent years has become a research hotspot of future power grid[1].With increasing concerns about energy saving technology and rapid development of power electronics, the renewable energy sources(RES) have been integrated into the smart grid on a large scale. Applications of RES hold advantages in low distribution loss, improved power quality, and high reliability[2]. The sources of the renewable energy include wind power, PV power, fuel cell batteries, etc. Photovoltaic (PV) power has been a promising renewable energy source due to its ability to operate with much less restriction on location, and ease of maintenance [3]. Nowadays, the grid-connected PV system has become an important means of PV power utilization [4].

To integrate the various energy sources into the utility grid, power electronic devices are vital to match the voltage levels between RES and grid, deliver the power and meet the power quality requirements of grid. Grid-connected voltage source inverters (VSIs) have been widely used to integrate renewable energy sources to the utility network [5]-[10]. Coupling inductors are connected between the inverter and the grid for smoothing the output of the pulse width modulated (PWM) VSI and reducing the current ripples. This kind of VSI is named inductive-coupling VSI in this paper, as shown in Fig.1. In order to inject active power from the renewable energy sources to the grid, the output voltage of the inverter needs to be higher than the grid voltage at the point of common coupling (PCC). Some researchers control the inductive-coupling VSIs to achieve active power transfer, reactive power compensation and harmonic compensation simultaneously [9][10]. However, the reactive power and harmonics compensation requires the voltage of the VSI increasing to an even higher value. As a consequence, the total system cost and operational losses increase.

Instead of the inductor, the coupling branch can be set to capacitive at fundamental frequency, which is usually constructed by a capacitor and an inductor. This kind of grid-connected VSI is named capacitive-coupling VSI, as shown in Fig.2.

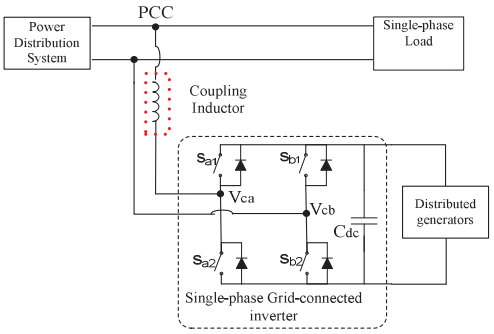

Figure 1 Inductive-coupling VSI

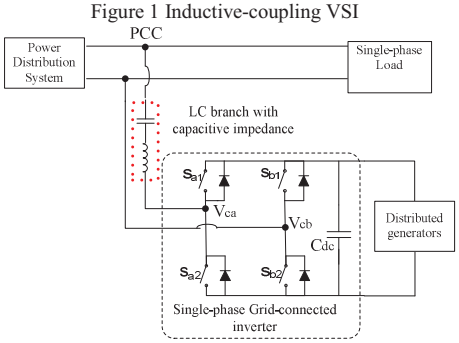

Figure 2 Capacitive-coupling VSI

When reactive power is injected for compensating inductive loads, the capacitive-coupling VSI can achieve the compensation with the dc bus voltage much lower than the system voltage. Many previous works have analyzed this and low cost hybrid power filters were proposed [11]-[13]. When the grid-connected inverter is used to transfer the active power from the distributed generators and compensate the reactive power at PCC, to apply the capacitive-coupling VSI may provide a low-cost alternative compared to the inductive-coupling VSI. Hence, a capacitor-coupling VSI for PV integration is studied and implemented in this paper.

The inductive-coupling and capacitive-coupling VSIs are studied and compared in section II. In Section III, a power conversion system for the PV panels are implemented by using the capacitive-coupling VSI and a boost-half-bridge dc/dc converter. The boost-half-bridge dc/dc converter is adopted to achieve galvanic isolation and maximum point power tracking(MPPT). The system configuration and the control system are presented in this section. Simulation results are provided in Section IV. Comparison with an inductive-coupling VSI is also done in Section IV. The conclusion is given in the last Section.

II. COMPARISONS OF INDUCTIVE-COUPING VSI AND CAPACITIVE-COUPLING VSI

The inductive-coupling VSI and capacitive-coupling VSI are first compared. When these two inverters serve as the grid-connected inverter in smart grid, they need to inject active power to the grid in some applications. For example, to integrate distributed generators to the grid, such as PV generators, battery energy storage system. The power control capability of the two grid-connected VSIs are studied and compared hereinafter.It is assumed active power and reactive power are transferred simultaneously. The injecting current from the VSI to the grid is expressed as:

$$I_{cf} = I_{cfp} + j\, I_{cfq}, \tag{1}$$

where I_{cfp} is in phase with voltage at the PCC; it inject or absorb active power from the grid. I_{cfq} is perpendicular to the voltage, which correpsonds to the reactive power.

The equivalent circuit for the inductive-coupling VSI is shown in Fig. 3 (a), in which the VSI is modeled by a voltage source. The corresponding voltage drop across the coupling inductor is:

$$\vec{V}_{Lf} = \vec{I}_{cf} \cdot (jX_L) \tag{2}$$

The voltage vector is the current vector rotates 90 degree counter clockwise. The output voltage of the VSI is calculated as:

$$\vec{V}_{invLf} = \vec{V}_S + \vec{V}_{Lf} = \vec{V}_S + \vec{V}_{qLf} + \vec{V}_{pLf} \quad . \tag{3}$$

where $V_{qLf} = X_L * I_{cfq,}$, $V_{pLf} = X_L * I_{cfp}$ and V_s is the grid side voltage. The corresponding phasor diagram is shown in Fig. 3(b).

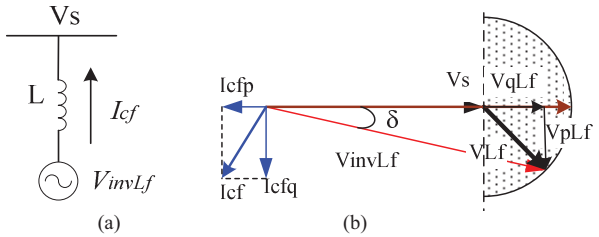

Fig. 3 Inductive-coupling VSI (a) Equivalent circuit (b) Phasor diagram

The equivalent circuit for the capacitive-coupling VSI is shown in Fig. 4 (a). The capacitor is the equivalent impedance of the *LC* coupling circuits under the fundamental frequency. The corresponding voltage drop across the coupling capacitor is:

$$\vec{V}_{Cf} = \vec{I}_{cf} \cdot (-jX_C) \tag{4}$$

The voltage vector is the current vector rotates 90 degree clockwise. The output voltage of the inverter is:

$$\vec{V}_{invcf} = \vec{V}_S + \vec{V}_{Cf} = \vec{V}_S + \vec{V}_{qcf} + \vec{V}_{pcf} \tag{5}$$

where $V_{qcf} = X_c * I_{cfq,}$, $V_{pcf} = X_c * I_{cfp}$.The corresponding phasor diagram is shown in Fig. 4(b)

The selected current vector in these two figures indicate active power is injected to the grid and reactive power is for compensting inductive loads. It is evident that the capacitive-coupling VSI is able to control the power flow with a lower output voltage under this circumstance. In order to compare the power control capability of the two grid-connected inverters, the power flow between the VSI and the grid is given in Eqs. (6)and (7) [14].

$$P_{inj} = \left(\frac{V_S^2}{z} - \frac{V_S V_{inv}}{z}\cos\delta\right)\cos\theta - \frac{V_S V_{inv}}{z}\sin\delta\cdot\sin\theta \tag{6}$$

$$Q_{inj} = \left(\frac{V_S^2}{z} - \frac{V_S V_{inv}}{z}\cos\delta\right)\sin\theta + \frac{V_S V_{inv}}{z}\sin\delta\cdot\cos\theta \tag{7}$$

where V_S is the grid voltage, V_{inv} is output voltage of the VSI, phase angle δ is the phase difference between grid voltage V_S and inverter output voltage V_{inv}, Z and θ is the amplitude and angle of the coupling impedance. The power base are defined as Eqs. (8) and (9).

$$S_{base} = V_S^2 / \omega L \tag{8}$$

$$S_{base} = V_S^2 \omega C \tag{9}$$

where L, C indicte the coupling impedance and ω represents the grid frequency. The power flow in per unit form is deduced from Eqs. (6) to (7), as given in Eqs. (10) and (11). The power flow control capability of the two VSIs are compared based on thest two equations.

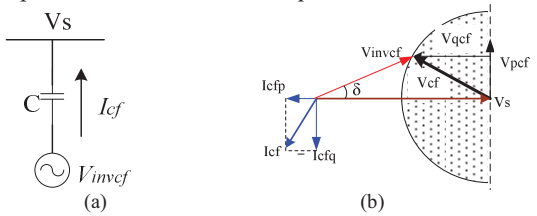

Fig. 4 Capacitive-coupling VSI (a) Equivalent circuit (b) Phasor diagram

$$P_{inj}/S_{base} = \left(1 - \frac{V_{inv}}{V_S}\cos\delta\right)\cos\theta - \frac{V_{inv}}{V_S}\sin\delta\cdot\sin\theta \quad (10)$$

$$Q_{inj}/S_{base} = \left(1 - \frac{V_{inv}}{V_S}\cos\delta\right)\sin\theta + \frac{V_{inv}}{V_S}\sin\delta\cdot\cos\theta \quad (11)$$

The variations of the power flow are shown in Figs.5 and 6. According to the direction of the current in Figs. 3 and 4, the active power is negative when power is injected to the grid. The reactive power is negative when reactive power is injected for compensating inductive loads. The horizontal axis in these two figures is the phase angle δ between grid voltage V_S and inverter output voltage V_{inv}. The angle θ is 90 degree for the inductive-coupling VSI and is -90 degree for the capacitive-coupling VSI. The active power in (10) is odd symmetrical of δ and the reactive power in (11) is even symmetrical of δ. As a result, half range of δ is showed, in which active power is injected to the grid.

The variations of the active power flow in Figs. 5 and 6 are the same. When the magnitude and angle of the VSI output voltage is determined by the active power flow, the reactive power is determined accordingly. It is clear in Fig. 5 that the inductive-coupling VSI can only inject reactive power for compensating capacitive loads when its voltage rating is smaller than the grid voltage. On the contrary, the capacitive-coupling VSI can compensate inductive loads when its voltage rating is smaller than the system voltage, as shown in Fig.6. Hence, the capacitive-coupling VSI is able to inject active power to the power system when it also compensates reactive power from inductive loads at the PCC. The reduced voltage rating of the VSI can reduce the initial cost and the operational losses.

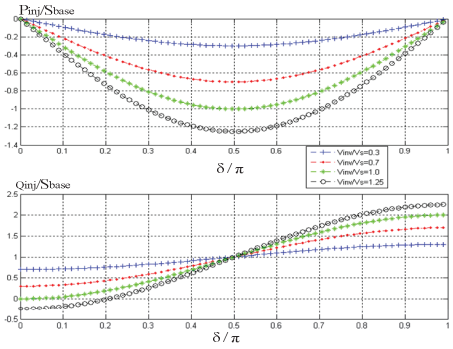

Fig.5 Power flow of the inductive-coupling VSI

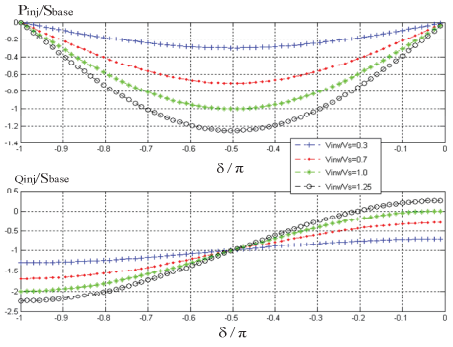

Fig.6 Power flow of the capacitive-coupling VSI

III. CAPACITIVE-COUPLING VSI FOR PV INTEGRATION

A. PV Integration system and its control block diagram

The characteristic of the power flow of the capacitive-coupling VSI is analyzed. In this section, the PV integration system using capacitive-coupling VSI is implemented. The reactive compensation is achieved simultaneously by the system together with the active power transfer. The system configuration is shown in Fig.7, which consists of PV panels, boost-half-bridge dc-dc converter, VSI and the capacitive-coupling branch.

The corresponding control block diagram of the whole system is shown in Fig.8. The output voltage of PV panel V_{PV}, dc-link voltage V_{dc} , the grid voltage V_S are sensed, the output current of PV panel I_{PV}, the inverter output current i_c and the load current i_L are measured and sent to the controller. The boost-half-bridge dc-dc converter achieves the MPPT by the adaptive duty cycle control algorithm [15]. The active power from the PV is transferred to the grid and reactive power of the inductive loads is compensated. The power balance of the whole system is controlled by keeping the dc-link voltage stable.

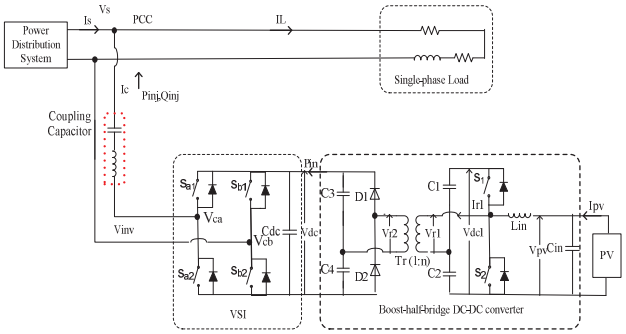

Fig.7 System Configuration of Capacitive-coupling VSI

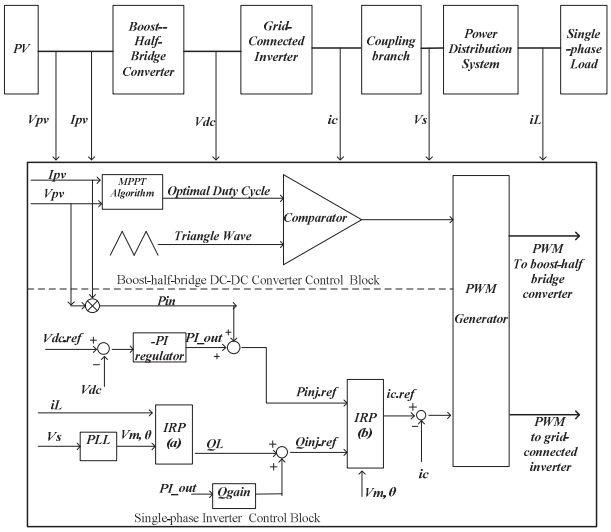

Fig.8 Control block diagram of the PV integration system with capacitive-coupling VSI

B. Boost-half-bridge dc-dc converter and MPPT

The circuit of boost-half-bridge converter is shown in Fig.7 [16]. In the boost-half-bridge dc–dc converter, C_{in} and L_{in} denote the input capacitor and boost inductor, respectively. The center taps of the two MOSFETs (S_1 and S_2) and the two output capacitors (C_1 and C_2) are connected to the primary terminals of the transformer T_r , just similar to a half bridge. The transformer leakage inductance reflected to the primary is represented by L_s and the transformer turns ratio is 1 : n. A voltage doubler composed of two diodes (D_1 and D_2) and two capacitors (C_3 and C_4) is incorporated to rectify the transformer secondary voltage to the inverter dc link. Other symbol representations are defined as follows. The duty cycle of S_1 is denoted by d_1 . The low-voltage side (LVS) dc-link voltage is V_{dc1} and the high voltage side (HVS) dc-link voltage is V_{dc}.The boost-half-bridge converter is controlled by S_1 and S_2 with complementary duty cycles. Neglect all the switching dead bands for simplification [17].Therefore, (12) and (13) can be derived as follows:

$$V_{dc1} = \frac{V_{PV}}{d_1} \tag{12}$$

$$V_{dc} = n * \frac{V_{PV}}{d_1} \tag{13}$$

The boost-half bridge converter boosts the dc voltage identically as a conventional boost converter, but with the extra features of the galvanic isolation as well as the high step-up ratio. The simple circuit topology with minimal use of semiconductor devices exhibits a low total cost and good reliability [17].

The maximum power point tracking (MPPT) process [18][19] is based on the gradient approximation. Gradient approximation is a stochastic optimization method, which is used for extracting maximum power from PV generation system. The detailed control block diagram of gradient approximation process is shown in Fig.9 [15].The MPPT control loop runs again and again until the optimal duty cycle is achieved to drive the dc-dc converter to reach the maximum power point of the PV panels.

C. Control of the capacitive-coupling VSI

The average reactive power required by the inductive loads at the PCC is selected as the power base for designing the capacitive-coupling VSI. Based on (9), the coupling impedance at the fundamental frequency is denoted as X_C, which is calculated by [20]:

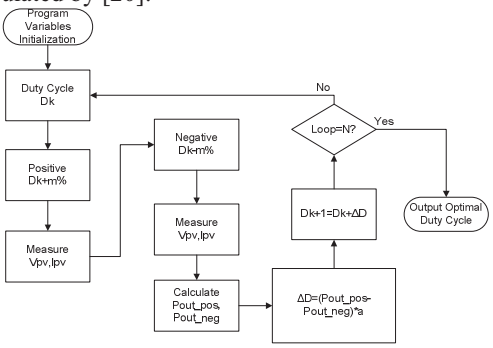

Fig.9 MPPT control block diagram.

$$X_C = V_S^2 / S_{base} = V_S^2 / Q_{average} \tag{14}$$

The inductor is then selected to reduce current ripples. The capacitive-coupling VSI is controlled to achieve simultaneous active and reactive power control. The minimum dc-link voltage is calculated based on the reactive power and active power to be transferred as follows:

$$V_{dc.min} = \sqrt{2} * \sqrt{(1-\frac{Q_{inj}}{S_{base}})^2 + (\frac{P_{source}}{S_{base}})^2} * V_s \tag{15}$$

where Q_{inj} is reactive power to improve grid side power factor and P_{source} is the active power from the PV system.

Fig.8 shows the control system of the capacitive-coupling VSI. Power balance of the inverter is achieved through the dc-link voltage regulator, which is implemented by a negative PI controller. The sum of the active power generated from PV system and the output of the PI-controller is the final active power for extracting the reference currents. The reactive power of the loads are extracted by instantaneous reactive power (IRP) module IRP(a). Current reference is obtained from the module IRP(b). The hysteresis pulse width modulation is adopted for the current tracking with fast dynamics.

IV. Simulation Results

A.Comparison of inductive-coupling VSI and capacitive-coupling VSI

The inductive-coupling VSI and capacitive-coupling VSI, as grid-connected inverter to transfer active and reactive power, are first compared. To simplify the system configuration, the dc-link of the two VSIs is supplied by a constant dc source. Simulation verifications are carried out in PSCAD/EMTDC. In the simulation, the loads are modeled by a parallel combination of a resistor and a series-connected branch of an inductor. The system parameters are listed in Table 1. The dc-link voltage of the inductive-coupling VSI is 330V in the simulation; while the dc-link voltage of the capacitive-coupling VSI is 71V.

The simulation results of the two VSIs are shown in Figs. 10 and 11. The I_s and I_{load} denote the source current and load current. The variables $P_{source,}$ $P_{inj,}$ $Q_{inj,}$ Q_{load} indicate active power reference, the active power transferred to the grid, the reactive power transferred to the grid and the reactive power of loads, respectively. The detailed system parameters are given in Table 2.

TABLE 1 SYSTEM PARAMETERS IN THE SIMULATION VERIFICATION

Grid voltage Vs	220 V
DC-link Voltage	Inductive-coupling VSI: 330V
	Capacitive-coupling VSI: 71V
Sampling frequency	20kHz
Source inductor Ls	0.002 mH
Inductive-coupling VSI:	Coupling inductor: 7mH
Capacitive-coupling VSI	Coupling Inductor: 7.5mH
	Coupling Capacitor: 54uF
Linear load	120ohm; 0.17H, 17ohm

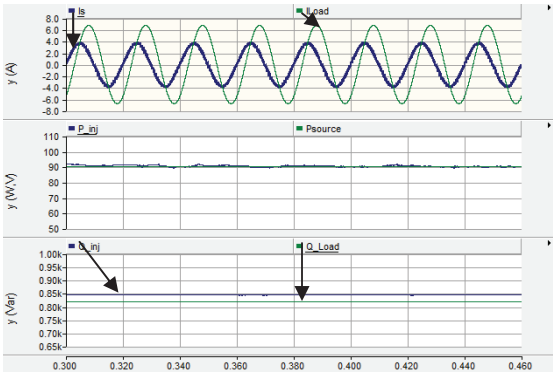

Fig.10 Simulation results of inductive-coupling VSI

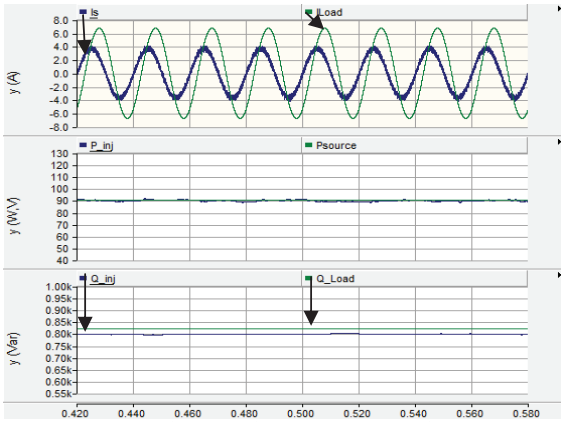

Fig.11 Simulation results of capacitive-coupling VSI

TABLE 2 COMPARISONS OF PERFORMANCES BETWEEN THE INDUCTIVE-COUPLING VSI AND CAPACITIVE-COUPLING VSI

Performance Indexes	Load	Performance of grid-connected VSI Grid-side	
		Inductive-coupling	Capacitive-coupling
Active power	661W	571W	571W
Power Factor	0.63	1.00	1.00
Current RMS	4.83A	2.62A	2.62A
Current THD	/	4.53%	3.49%

In the simulation, the inductive-coupling VSI and capacitive-coupling VSI are controlled to inject the same amount of active and reactive power to the grid. Results indicate that the dc-link voltage of the capacitive-coupling VSI is lower than 1/4 of the inductive-coupling VSI when the same power is transferred. As a result, the initial cost and operational losses are greatly reduced by adopting the proposed capacitive-coupling VSI.

B. The PV integration system

In this section, the proposed PV integration system with capacitive-coupling VSI is tested. The system configuration is shown in Fig. 7. The equivalent circuit of a PV cell is shown in Fig.12[21].*V–I* characteristic curve and *P–V* characteristic curve of PV model is depicted in Fig.13(a) and Fig.13 (b). From the P-V characteristic curve, it can be found that the maximum power point is located at about P_m=55.4W,V_m=32.1V.

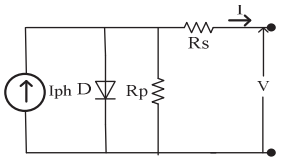

Fig.12 Equivalent model of the PV panel

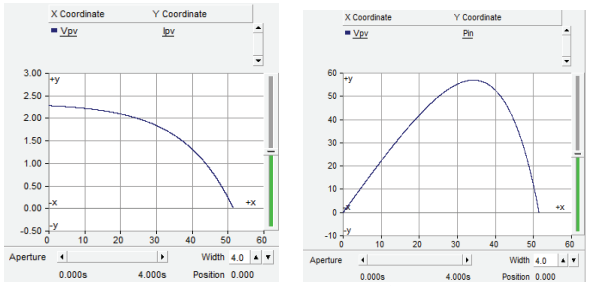

(a)V-I (b)P-V

Fig.13 Power characteristics curve of PV panel

The MPPT is applied to control the duty-cycle of the power switches at the input stage of the dc-dc converter. The output P-V curve of the PV model is shown in Fig.14(a) and the duty cycle of the upper power switch is shown in Fig. 14(b). The output power approaches the maximum power point P_m=55.4W and is kept at this operating point. The V_{dc_ref}, V_{pv} and V_{dc} denote the dc-link reference voltage ,the input voltage of dc-dc converter and the dc-link voltage. The current waveform and dc-link voltage are shown in Fig.15. It can be seen that the dc-link voltage is controlled to the minimum dc-link reference voltage and keeps stable in steady state. Meanwhile, the active power from the PV model is transferred to the grid and the reactive power is compensated simultaneously. Detailed results are also listed in Table 3.

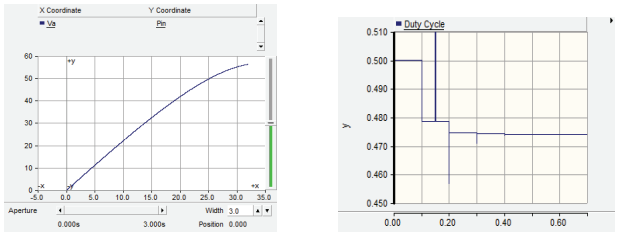

(a) P–V curve of MPPT process (b) Duty cycle status of MPPT process

Fig.14 the output P–V curve of PV panel with MPPT method.

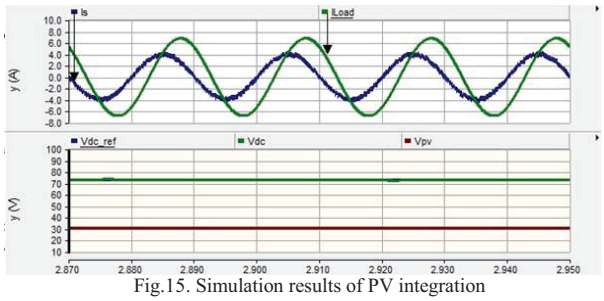

Fig.15. Simulation results of PV integration

TABLE 3 PERFORMANCE OF CAPACITIVE-COUPLING VSI FOR PV INTEGRATION

Performance Indexes	Load	Grid Side
Active power	665W	610W
Power Factor	0.63	0.99
Current RMS	4.85A	2.81A
Current THD	/	3.35%

VI. CONCLUSIONS

A capacitive-coupling VSI for grid-connected PV systems has been presented in this paper. Based on the comparisons between the inductive-coupling VSI and the capacitive-coupling VSI, the capacitive-coupling VSI is a low-cost alternative to the existing grid-connected inverter, which is able to transfer the active power and compensate the reactive power with much lower inverter voltage rating. A low dc-link PV integration system is implemented, in which a boost-half-bridge dc–dc converter is used to achieve MPPT and galvanic isolation. Simulation results are provided to verify the validity of the capacitor-coupling VSI for PV integration and its control algorithm. To transfer the same amount of power, the dc-link voltage of the capacitive-coupling VSI is lower than 1/4 of the dc-link voltage of the inductive-coupling VSI.

ACKNOWLEDGMENTS

The authors would like to thank the Science and Technology Development Fund, Macao SAR Government with the project (072/2013/A3), University of Macau with the project (MYRG135(Y2-L2)-FST11-DNY) and Shanghai City Natural Science Foundation (Contract No.: 13ZR1422800) for their support.

REFERENCES

[1] Xiang Yuan, ZhenXing Qian, Yang Zhou, "Discussion on the development trend of smart grid and its key technology" 2012 China International Conference on Electricity Distribution, 5-6 Sep. 2012,pp.5-6.

[2] Tsai-Fu Wu, Hung-Shou Nien, Hui-Ming Hsieh, and Chih-Lung Shen, "PV Power Injection and Active Power Filtering With Amplitude-Clamping and Amplitude-Scaling Algorithms", *IEEE Transactions on Industry Applications*, VOL. 43, NO. 3, MAY/JUNE 2007, pp. 731-741.

[3] M. J. V. Vazquez, J. M A. Marquez, and F. S. Manzano, "A methodology for optimizing stand-alone PV-System sizing using parallel-connected dc/dc converter," *IEEE Trans. Ind. Electron*., vol. 55, no. 7, pp. 2664–2673, Jul. 2008.

[4] T. Kerekes, R, Teodorescu, M. Liserre, C. Klumpner, and M. Sumner, "Evaluation of three-phase transformerless photovoltaic inverter topologies," *IEEE Trans. Power Electron*., vol. 24, no. 9, pp. 2202–2211, Sep.2009.

[5] W. Wu, Y. He, and F. Blaabjerg, "An LLCL power filter for single-phase grid-tied inverter," *IEEE Trans. Power Electron*., vol. 27, no. 2, pp. 782– 789, Feb. 2012.

[6] H. J. Avelar, W. A. Parreira, J. B. Vieira, L. C. G. de Freitas, and E. A. A. Coelho, "A state equation model of a single-phase grid-connected inverter using a droop control scheme with extra phase shift control action," *IEEE Trans. Ind. Electron*., vol. 59, no. 3, pp. 1527–1537, Mar. 2012.

[7] S. H. Hwang, L. Liu, H. Li, and J. M. Kim, "DC offset error compensation for synchronous reference frame PLL in single-phase grid-connected converters," *IEEE Trans. Power Electron*., vol. 27, no. 8, pp. 3467–3471, Aug. 2012.

[8] T. F. Wu, C. L. Kuo, K. H.. Sun, Y. K. Chen, Y. R. Chang and Y. D. Lee, " Integration and operation of a single-phase bidirectional inverter with two buck/boost MPPTs for DC-distribution applications", *IEEE Trans. Power Electron.*, Vol. 28, no. 11, pp. 5098-5106, 2013.

[9] R. I. Bojoi, L. R. Limongi, D. Roiu and A. Tenconi, "Enhanced Power Quality Control Strategy for Single-phase Inverters in Distributed Generation Systems", *IEEE Trans. Power Electro*.,Vol.26, pp. 798-806, 2011.

[10] D. M. Soto and C. S. Edrington, "Mitigation of PHEV Charging Impact on Transformers via a PV-APF Harmonic Compensation Technique: Application to V2G Integration", *Proc. of IEEE Vehicle Power and Propulsion Conference*, 2011, pp. 1-5.

[11] H. Akagi and K. Isozaki, "A hybrid active filter for a three-phase 12-pulse diode rectifier used as the front end of a medium-voltage motor drive", *IEEE Trans. Power Electro*.,Vol.27, No.1, pp. 69-77, Jan. 2012.

[12] C.S. Lam, W. H. Choi, M. C. Wong and Y. D. Han, "Adaptive DC-link voltage-controlled hybrid active power filters for reactive power compensation", *IEEE Trans. Power Electro*., Vol. 27, No.4, pp. 1758-1772, 2012.

[13] C. S. Lam, M. C. Wong and Y. D. Han, "Hysteresis current control of hybrid active power filters", *IET Power Electronics*, Vol.5, pp. 1175-1187, 2012.

[14] J. M. Guerrero, J. Matas, L. G. Vicua, Miguel Castilla, and Jaume Miret, "Wireless-Control Strategy for Parallel Operation of Distributed-Generation Inverters", *IEEE Trans. Industrial Electronics* , Vol. 53, pp. 1461-1470, 2006.

[15] Ying-Yi Hong, Shiue-Der Lu, Ching-Sheng Chiou, "MPPT for PM wind generator using gradient approximation ", *Energy Conversion and Management,* Vol. 50, Issue 1, Jan. 2009, Pages 82 – 89

[16] F. Z. Peng, H. Li, G. Su, and J. S. Lawler, "A new ZVS bidirectional DC– DC converter for fuel cell and battery application," *IEEE Trans. Power Electron.*, vol. 19, no. 1, pp. 54–65, Jan. 2004.

[17] Shuai Jiang, Dong Cao, Yuan Li, Fang Zheng Peng, "Grid-Connected Boost-Half-Bridge Photovoltaic Microinverter System Using Repetitive Current Control and Maximum Power Point Tracking" *IEEE Trans. Power Electron*., Vol. 27, no. 11,pp.4712-4721, Nov. 2012

[18] A. K. Abdelsalam, A. M. Massoud, S. Ahmed, and P. N. Enjeti, "High-performance adaptive perturb and observe MPPT technique for photovoltaic-based microgrids," *IEEE Trans. Power Electron*., vol. 26, no. 4, pp. 1010–1021, Apr. 2011.

[19] G. C. Hsieh, H.-L. Chen, Y. Chen, C.-M. Tsai, and S.-S. Shyu, "Variable frequency controlled incremental conductance derived MPPT photovoltaic stand-along DC bus system," *in Proc. APEC, 2008*, vol. 23, pp. 1849–1854.

[20] Wen-Chen Zhang, Ning-Yi Dai, Man-Chung Wong, Chi-Kong Wong, "Capacitive-coupled grid-connected inverter with active power injection ability", *in Proc. of ECCE (Asia) 2012*, pp. 1-7.

[21] Moacyr Aureliano Gomes de Brito, Luigi Galotto, Jr., Leonardo Poltronieri Sampaio, uilherme de Azevedo e Melo, and Carlos Alberto Canesin, "Evaluation of the Main MPPT Techniques for hotovoltaic Applications" *IEEE Trans. on Industry Electronics*, Vol. 60, no. 3, pp:1156-1167,March 2013